

Mask2Lesion: Mask-Constrained Adversarial Skin Lesion Image Synthesis

Kumar Abhishek and Ghassan Hamarneh

School of Computing Science, Simon Fraser University, Canada
`{kabhishe,hamarneh}@sfu.ca`

Abstract. Skin lesion segmentation is a vital task in skin cancer diagnosis and further treatment. Although deep learning based approaches have significantly improved the segmentation accuracy, these algorithms are still reliant on having a large enough dataset in order to achieve adequate results. Inspired by the immense success of generative adversarial networks (GANs), we propose a GAN-based augmentation of the original dataset in order to improve the segmentation performance. In particular, we use the segmentation masks available in the training dataset to generate new synthetic skin lesion images using a conditional GAN, modeling this as a paired image-to-image translation task, which are then used to augment the original training dataset. We test Mask2Lesion augmentation on the ISBI ISIC 2017 Skin Lesion Segmentation Challenge dataset and observe that it improves the segmentation accuracy, compared to a model trained with only classical data augmentation techniques by 1.12%.

Keywords: skin lesion · generative adversarial networks · image segmentation.

1 Introduction

Melanoma, a type of skin cancer, although represents a small fraction of all skin cancers in the USA, accounts for over 75% of all skin cancer related fatalities [16]. In fact, melanoma is responsible for over 10,000 deaths annually in the USA alone [1]. However, studies have shown that the survival rates of patients improves drastically with early diagnosis. Skin lesion segmentation is a crucial step in the diagnosis and subsequent treatment of melanoma. Segmentation refers to the process of localization and delineation of the lesion boundary in order to separate it from the surrounding skin. Although several core methods such as the 7-point checklist [11], the ABCD (Asymmetry, Border, Color, and Differential structure) rule [13], and the CASH (Color, Architecture, Symmetry, and Homogeneity) algorithm [8] have been developed by dermatologists to diagnose melanoma, their performance has been sub-optimal. This motivates the use of deep learning based computer-aided diagnosis systems to improve the accuracy and sensitivity of melanoma detection methods.

Recent works on skin lesion segmentation using deep learning have shown significant improvements in segmentation accuracy. Yuan et al. [21] used a 19-layer deep fully convolutional network with a Jaccard distance based loss function that is trained end-to-end to segment skin lesions. Mirikharaji et al. [12] proposed a deep auto-context architecture to use image appearance information along with the contextual information to improve segmentation results. Yu et al. [20] proposed using a deep residual network architecture with several blocks stacked together to improve the representative capability of the network and therefore increase the segmentation accuracy.

Generative adversarial networks (GANs), proposed by Goodfellow et al. [6] have been immensely popular in realistic image generation tasks. Numerous variations of these generative models have been developed for a variety of applications, including text to image synthesis and video generation [15,18]. GANs have also been used, with varying degrees of success, to generate medical images. Frid-Adar et al. [5] used GANs to generate liver lesion images to augment the training dataset in an attempt to improve the lesion classification accuracy. Wolterink et al. [19] used CycleGAN [22] to generate brain CT images from corresponding brain MR images. Recently, GANs have also been applied to skin lesion synthesis - Baur et al. [2] made modifications to state-of-the-art GANs to generate high resolution (256×256 pixels) skin lesion images. Bissoto et al. [3] modeled skin lesions using semantic label maps and superpixels, and evaluated three GAN architectures for skin lesion synthesis. Pollastri [14] modified two GAN architectures to generate skin lesions along with their corresponding segmentation masks.

In this work, we propose to use the lesion boundaries to generate synthetic lesion images in order to augment the training dataset and improve skin lesion segmentation performance. Isola et al. [9] and Zhu et al. [22] have shown that it is possible to generate high resolution realistic images from sketches. An inherent advantage of using lesion boundaries to generate skin lesion images is that the newly generated images can be used for training the segmentation network without needing to be annotated. To the best of our knowledge, this is the first work that uses GANs to synthesize skin lesion images from lesion boundaries.

The rest of the paper is structured as follows: we discuss the proposed approach in Section 2, we describe the dataset and experimental details in Section 3, we analyze the quantitative and qualitative results of our proposed approach in Section 4, and Section 5 concludes the paper.

2 Method

2.1 Method Overview

The purpose of our method is to synthesize segmentation training data which is then used to augment the existing data for training a segmentation network. We model this as an image-to-image translation task where we train a deep neural network model, called Mask2Lesion, to generate the synthetic data. In particular, we translate images containing binary segmentation masks, which highlight

the area of a target skin lesion, to a skin image containing a lesion confined to that binary mask, making it a paired image-to-image translation task. To this end, we train a network with paired skin lesion images and their corresponding masks. Such training data is also one typically provided for training segmentation methods. Our deep network is based on pix2pix architecture which comprises of a conditional generative adversarial network (GAN), described in Section 2.3. With the ability to translate a binary mask to a corresponding image containing a lesion delineated by the mask, we can then turn our attention to creating synthesized masks (via different approaches), and rely on our trained Mask2Lesion model to generate the images. Given a training dataset of images and segmentation masks, with or without augmentation (performed using Mask2Lesion or otherwise), we can then train a segmentation network. The segmentation network used here is described in Section 2.4.

2.2 Segmentation Masks

We propose to use lesion segmentation masks as input to the generative algorithm, making it easy to produce a large number of inputs. Since the ISIC 2017 Skin Lesion Segmentation dataset [4] used for the segmentation task has ground truth segmentation masks available, they can be used as inputs to the generative algorithm to synthesize skin lesions, thus creating new pairs of lesion images and their masks. Figure 1 shows four sample lesion image with their corresponding segmentation masks.



Fig. 1: A few sample images from the ISIC training dataset along with the corresponding segmentation masks. Note the presence of artifacts in some of the images.

2.3 Image-to-Image Translation Network

The pix2pix image-to-image translation model proposed by Isola et al. [9] uses a conditional GAN to generate images. Unlike traditional GANs which learn a mapping from a random noise vector to an output image, conditional GANs learn a mapping from an observed image x and a random noise vector z to an

output image y . The two components of a conditional CycleGAN are a generator and a discriminator. The generator G is trained to produce output images, $G : \{x, z\} \rightarrow y$ which are “realistic”, meaning they cannot be distinguished from the original images. The discriminator D tries to distinguish between the original images and the output of the generator G . The two components can be estimated using deep neural networks. This conditional GAN is trained in an adversarial manner, and the objective function can be written as

$$\mathcal{L}_{cGAN}(G, D) = \mathbb{E}_{x,y} [\log D(x, y)] + \mathbb{E}_{x,z} [\log (1 - D(x, G(x, z)))] \quad (1)$$

where the generator G tries to minimize this objective function and the discriminator D tries to maximize it. The optimal solution is obtained using this minimax game

$$G^* = \arg \min_G \arg \max_D \mathcal{L}_{cGAN}(G, D). \quad (2)$$

This is different from an unconditional GAN where the discriminator D does not observe the input image x .

Generator Architecture Since the output of the generator shares the underlying structure with the input, an encoder decoder architecture with skip connections has been chosen as the generator. We use U-Net [17] with an L1 loss because in its attempt to fool the discriminator, L2 loss tends to produce more blurry generator outputs. The U-Net has a fully convolutional neural network architecture consisting of two paths - a contracting path and a symmetric expansive path. Skip-connections containing feature maps from the contracting path to the symmetrically corresponding layer’s upsampled feature maps in the expanding path assist recovery of the full spatial resolution at the network output [10].

Discriminator Architecture While using the L1 loss for the generator makes sure that the low frequency details are accurately captured, it is also important to model the high-frequency structure of the image. This is achieved by introducing a PatchGAN, a discriminator architecture which penalizes structure at local image patch level. As a result, the image is divided into several (overlapping) patches, each of which is labeled by the discriminator as ‘real’ or ‘fake’, and the overall output of the discriminator is the average of the individual responses.

Figure 2 shows a high level overview of the Mask2Lesion algorithm.

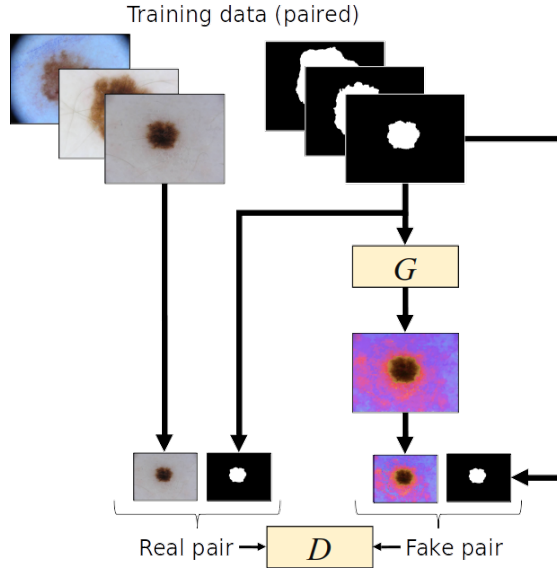


Fig. 2: The proposed Mask2Lesion algorithm.

2.4 Segmentation Network

Originally proposed by Ronneberger et al. [17] for the segmentation of neuronal structures in electron microscopic stacks, U-Net has been widely used for semantic image segmentation tasks - for natural as well as medical images. The U-Net consists of a fully convolutional encoder-decoder architecture with skip connections from layers in the encoder to the corresponding layers in the decoder, thereby leveraging information captured in the earlier layers to produce accurate delineations in the final output.

The contracting path consists of a repeated application of two 3×3 unpadded convolutions followed by a rectified linear unit (ReLU) non-linearity and a 2×2 max-pooling operation with a stride of 2. At each downsampling step, the number of feature channels is doubled. The expansive path consists of a 2×2 convolution of the feature map (“up-convolution”), at each stage of which the number of feature channels is halved. Moreover, the correspondingly cropped (to compensate for the loss of border pixels at every convolution) feature map from the contracting path is concatenated to this, and 2 convolutions with 3×3 are performed followed by a ReLU non-linearity. After this, a 1×1 convolution maps each 256-component feature vector to the desired number of classes, and the output is an image containing pixel-wise binary labels.

3 Data and Experimental Details

The dataset used for evaluation of the proposed approach was obtained from the 2017 ISBI ISIC Skin Lesion Analysis Towards Melanoma Detection: Lesion Segmentation Challenge [4]. There were 2000 training images and 150 test images. All the images and their corresponding ground truth segmentation masks were resized to 256×256 pixels using bilinear interpolation from the SciPy library.

The pix2pix model was trained for 200 epochs. For both the generator and the discriminator, all convolution operations used 4×4 spatial filters with a stride of 2. Each convolution layer (except the first) consists of convolution, batch normalization, dropout (with a keep probability of 0.5), and ReLU. The encoder (the contracting path of the U-Net) uses leaky ReLUs with a slope of 0.2, while the decoder (the expansive path) uses ReLUs. For the PatchGAN, a 70×70 patch is processed from the input image, which assigns a score to a 30×30 patch of the image. The patches overlap because the image sizes are 256×256 pixels. All network weights were sampled from a Gaussian distribution with zero mean and standard deviation of 0.02.

In order to evaluate the segmentation performance with and without GAN based augmentation, we train two segmentation networks - one with only the original dataset augmented with classical augmentation techniques (rotation, flipping, etc.) called ORIG, and the other with the original dataset augmented with classical as well as GAN based augmentation, called GAN-AUG.

For the two segmentation networks, we report three metrics - the Dice coefficient, the false positive rate (FPR), and the false negative rate (FNR).

4 Results and Discussion

Figure 3 (a) shows the output of Mask2Lesion when applied to segmentation masks from the ISIC dataset. We see that the synthesized lesions express variance in appearances and textures. We also test Mask2Lesion by using simple geometric shapes as masks, showing that synthesized images are well constrained by the mask boundaries (Figure 3 (b)). Furthermore, we test the adaptability of Mask2Lesion to hand-drawn masks. We draw two shapes - a large blob and a star shape, and then apply varying degrees of elastic deformations to them using DeformIt [7]. These masks are then used as inputs to Mask2Lesion and the corresponding outputs are shown in Figure 3 (c). We note that the goal for testing on geometric shapes and hand-drawn masks is to showcase our method's ability to generate skin lesion images confined to the input masks, even with complex or possibly unrealistic masks.

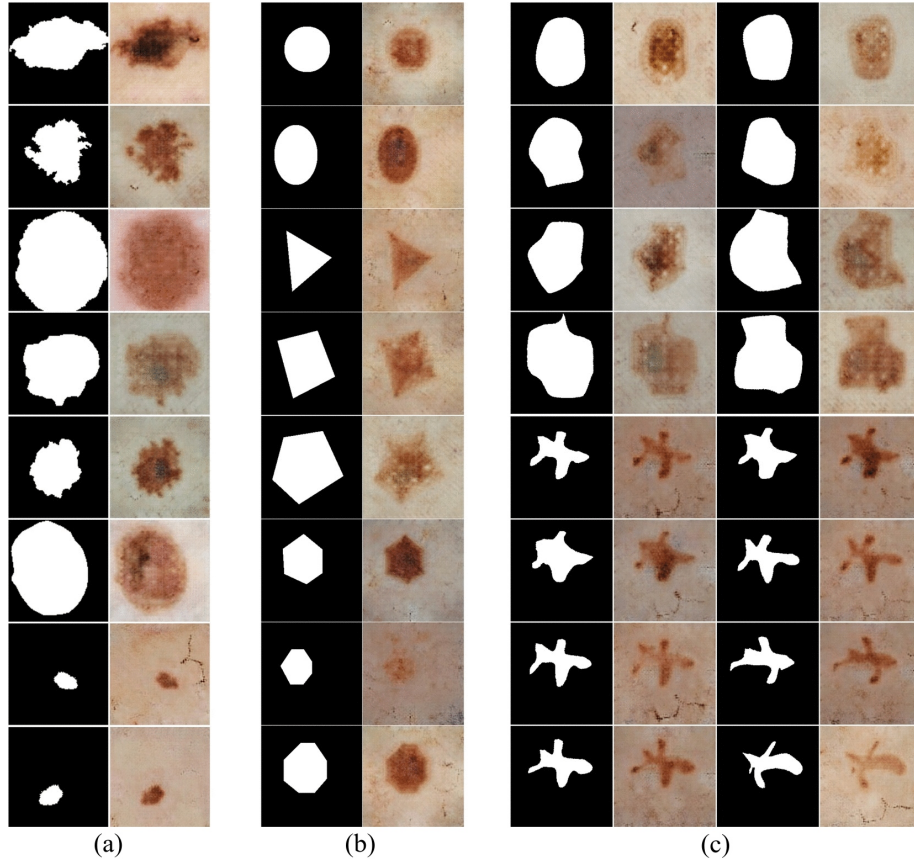


Fig. 3: (a) Segmentation masks from the ISIC dataset fed to Mask2Lesion and the corresponding generated lesion images. (b) Simple geometric shapes as masks and the corresponding outputs. (c) Elastic deformations applied to hand drawn masks using DeformIt and the corresponding synthesized lesion images.

Figure 4 shows samples from the test dataset for which the segmentation accuracy significantly improved with GAN-AUG. The outputs of GAN-AUG are much more closer to the ground truths and have fewer false positives as compared to ORIG. Table 1 shows the quantitative results for the 150 test images evaluated using the two methods. The proposed method achieves a 1.12% improvement in the mean Dice coefficient. There is also a noticeable improvement (i.e., decrease) in the false positive rate, although the false negative rate suffers a small deterioration.

In Figure 5, we plot the Gaussian kernel density estimates for the three metrics obtained for the test images for the two approaches, ORIG and GAN-AUG. The plots have been clipped to the range of values of the respective metrics and represent their probability distribution function estimates. The plots show

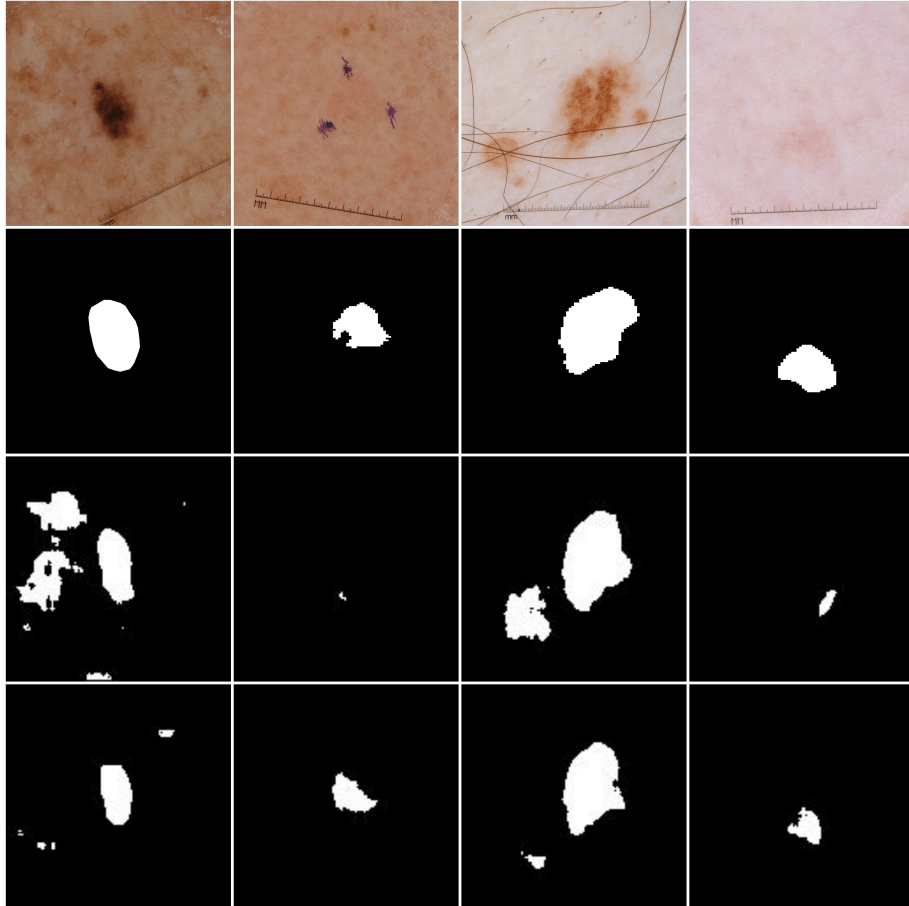


Fig. 4: Improved segmentation accuracy with the proposed method. The first row shows the test image samples, the second row shows the segmentation ground truths and the third and the fourth rows show the segmentations obtained from the ORIG and GAN-AUG respectively.

Table 1: Quantitative results for segmentation (Mean \pm Standard Error)

Method	Dice	FPR	FNR
ORIG	0.7743 ± 0.0202	0.0327 ± 0.0047	0.1906 ± 0.0222
GAN-AUG	0.7830 ± 0.0197	0.0174 ± 0.0032	0.2426 ± 0.0219

larger peaks corresponding to GAN-AUG as compared to ORIG at higher values of Dice coefficient. Moreover, the range of FPR values for GAN-AUG is lower than ORIG, meaning the proposed approach tends to mislabel pixels less frequently.

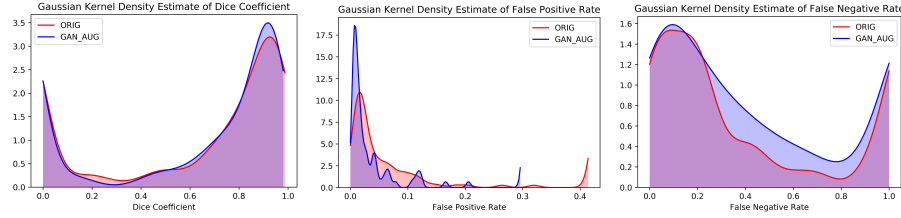


Fig. 5: Evaluating the proposed method - comparing Dice coefficient (left), false positive rate (middle), and false negative rate (right) for ORIG and GAN-AUG.

5 Conclusion

In this work, we proposed Mask2Lesion, a conditional GAN-based model to generate skin lesion images from and constrained to binary masks, and used these newly generated images along with their corresponding masks to augment the training dataset for improving the segmentation accuracy of skin lesion images. In particular, we used the segmentation masks from the original dataset as input to the generative algorithm so as to avoid the manual annotation of the newly synthesized skin lesion images. Our results showed an improvement in the segmentation accuracy when the training dataset for the segmentation network is augmented with these generated images.

References

1. Cancer facts & figures 2016, <https://www.cancer.org/research/cancer-facts-statistics/all-cancer-facts-figures/cancer-facts-figures-2016.html>
2. Baur, C., Albarqouni, S., Navab, N.: Melanogans: High resolution skin lesion synthesis with gans. arXiv preprint arXiv:1804.04338 (2018)
3. Bissoto, A., Perez, F., Valle, E., Avila, S.: Skin lesion synthesis with generative adversarial networks. In: OR 2.0 Context-Aware Operating Theaters, Computer Assisted Robotic Endoscopy, Clinical Image-Based Procedures, and Skin Image Analysis, pp. 294–302. Springer (2018)
4. Codella, N.C., Gutman, D., Celebi, M.E., Helba, B., Marchetti, M.A., Dusza, S.W., Kalloo, A., Liopyris, K., Mishra, N., Kittler, H., et al.: Skin lesion analysis toward melanoma detection: A challenge at the 2017 international symposium on biomedical imaging (isbi), hosted by the international skin imaging collaboration (isic).

In: Biomedical Imaging (ISBI 2018), 2018 IEEE 15th International Symposium on. pp. 168–172. IEEE (2018)

5. Frid-Adar, M., Klang, E., Amitai, M., Goldberger, J., Greenspan, H.: Synthetic data augmentation using GAN for improved liver lesion classification. In: Proceedings - International Symposium on Biomedical Imaging. vol. 2018-April, pp. 289–293. IEEE (apr 2018). <https://doi.org/10.1109/ISBI.2018.8363576>, <https://ieeexplore.ieee.org/document/8363576/>
6. Goodfellow, I., Pouget-Abadie, J., Mirza, M., Xu, B., Warde-Farley, D., Ozair, S., Courville, A., Bengio, Y.: Generative adversarial nets. In: Advances in neural information processing systems. pp. 2672–2680 (2014)
7. Hamarneh, G., Jassi, P., Tang, L.: Simulation of ground-truth validation data via physically-and statistically-based warps. In: International Conference on Medical Image Computing and Computer-Assisted Intervention. pp. 459–467. Springer (2008)
8. Henning, J.S., Dusza, S.W., Wang, S.Q., Marghoob, A.A., Rabinovitz, H.S., Polsky, D., Kopf, A.W.: The cash (color, architecture, symmetry, and homogeneity) algorithm for dermoscopy. *Journal of the American Academy of Dermatology* **56**(1), 45–52 (2007)
9. Isola, P., Zhu, J., Zhou, T., Efros, A.A.: Image-to-image translation with conditional adversarial networks. In: 2017 IEEE Conference on Computer Vision and Pattern Recognition (CVPR). pp. 5967–5976 (July 2017). <https://doi.org/10.1109/CVPR.2017.632>
10. Li, H., Xu, Z., Taylor, G., Studer, C., Goldstein, T.: Visualizing the loss landscape of neural nets. In: Advances in Neural Information Processing Systems. pp. 6389–6399 (2018)
11. Mackie, R., Doherty, V.: Seven-point checklist for melanoma. *Clinical and experimental dermatology* **16**(2), 151–152 (1991)
12. Mirikharaji, Z., Izadi, S., Kawahara, J., Hamarneh, G.: Deep auto-context fully convolutional neural network for skin lesion segmentation. In: Biomedical Imaging (ISBI 2018), 2018 IEEE 15th International Symposium on. pp. 877–880. IEEE (2018)
13. Nachbar, F., Stoltz, W., Merkle, T., Cognetta, A.B., Vogt, T., Landthaler, M., Bilek, P., Braun-Falco, O., Plewig, G.: The abcd rule of dermatoscopy: high prospective value in the diagnosis of doubtful melanocytic skin lesions. *Journal of the American Academy of Dermatology* **30**(4), 551–559 (1994)
14. Pollastri, F., Bolelli, F., Paredes, R., Grana, C.: Augmenting data with gans to segment melanoma skin lesions. *Multimedia Tools and Applications* (May 2019). <https://doi.org/10.1007/s11042-019-7717-y>, <https://doi.org/10.1007/s11042-019-7717-y>
15. Reed, S.E., Akata, Z., Yan, X., Logeswaran, L., Schiele, B., Lee, H.: Generative adversarial text to image synthesis. *CoRR* **abs/1605.05396** (2016), <http://arxiv.org/abs/1605.05396>
16. Rogers, H.W., Weinstock, M.A., Feldman, S.R., Coldiron, B.M.: Incidence estimate of nonmelanoma skin cancer (keratinocyte carcinomas) in the us population, 2012. *JAMA dermatology* **151**(10), 1081–1086 (2015)
17. Ronneberger, O., Fischer, P., Brox, T.: U-net: Convolutional networks for biomedical image segmentation. In: International Conference on Medical Image Computing and Computer-Assisted Intervention. pp. 234–241. Springer (2015)
18. Vondrick, C., Pirsiavash, H., Torralba, A.: Generating videos with scene dynamics. *CoRR* **abs/1609.02612** (2016), <http://arxiv.org/abs/1609.02612>

19. Wolterink, J.M., Dinkla, A.M., Savenije, M.H., Seevinck, P.R., van den Berg, C.A., Işgum, I.: Deep mr to ct synthesis using unpaired data. In: International Workshop on Simulation and Synthesis in Medical Imaging. pp. 14–23. Springer (2017)
20. Yu, L., Chen, H., Dou, Q., Qin, J., Heng, P.A.: Automated melanoma recognition in dermoscopy images via very deep residual networks. *IEEE transactions on medical imaging* **36**(4), 994–1004 (2017)
21. Yuan, Y., Chao, M., Lo, Y.: Automatic skin lesion segmentation using deep fully convolutional networks with jaccard distance. *IEEE Transactions on Medical Imaging* **36**(9), 1876–1886 (Sept 2017). <https://doi.org/10.1109/TMI.2017.2695227>
22. Zhu, J.Y., Park, T., Isola, P., Efros, A.A.: Unpaired image-to-image translation using cycle-consistent adversarial networks. *arXiv preprint* (2017)